Three-dimensional analysis of the rectifying properties of geometrically asymmetric metal-vacuum-metal junctions treated as an oscillating barrier

A. Mayer,[1,*] M. S. Chung,[2] B. L. Weiss,[3] N. M. Miskovsky,[4] and P. H. Cutler[4]

[1]*Laboratoire de Physique du Solide, Facultés Universitaires Notre-Dame de la Paix, Rue de Bruxelles 61, B-5000 Namur, Belgium*

[2]*Department of Physics, University of Ulsan, Ulsan 680-749, Republic of Korea*

[3]*Department of Physics, 130 CAC, The Pennsylvania State University, Altoona, Pennsylvania 16601, USA*

[4]*Department of Physics, 104 Davey Laboratory, The Pennsylvania State University, University Park, Pennsylvania 16802, USA*

(Received 1 August 2008; revised manuscript received 9 October 2008; published 4 November 2008)

We study the rectification properties of geometrically asymmetric metal-vacuum-metal junctions treated as an oscillating barrier. In particular, we focus on systems in which an oscillating bias is established between a cathode characterized by a hemispherical protrusion and a flat anode. We propose a quantum-mechanical approach of this problem by using a transfer-matrix methodology, with developments that enable the time dependence of the external bias to be accounted for explicitly. This study extends the quasistatic analysis presented in our previous work. In particular, we study how the rectification properties of these junctions depend on the frequency and the amplitude of the oscillating barrier. We also determine the power this device could provide to an external load and the efficiency, with which the energy of an incident radiation can be converted into a useful dc. It is demonstrated that rectification of optical frequencies is possible by using the nanoscale device discussed in this paper.

DOI: 10.1103/PhysRevB.78.205404 PACS number(s): 73.40.Ei, 85.30.Kk, 79.70.+q, 03.65.Nk

I. INTRODUCTION

Point-contact diodes were originally designed as metal-oxide-metal systems, in which one of the metals is essentially flat while the other has an extended sharp tip.[1] These diodes have been used for detection, rectification, and the frequency mixing of infrared radiation.[2–4] Fundamental applications have included the determination of the speed of light[5,6] and attempts to measure tunneling times.[7–11] Point-contact diodes have also enabled accurate measurements of infrared frequencies.[12–14] These devices are nowadays essentially used for the selective detection and mixing of infrared radiations, and current efforts aim at reducing their characteristic response times and at improving their sensitivity.[15–17]

An explanation of the rectification properties of these devices in terms of their geometrical asymmetry was proposed by Lucas *et al.*[18] in 1977.[10,19] The fact that an ac bias applied to these systems can induce currents with a strong dc component comes from the difference in the potential barrier seen by electrons traveling in the forward versus the backward directions. A cutoff of this rectification is expected when the frequency is so high that the bias reverses before the electron has been able to transit through the device.[9,10] Since tunneling times are typically of the order of 10^{-15} s,[9–11] this cutoff may appear at frequencies as high as 10^{15} Hz if the cathode-anode spacing is sufficiently small. These devices could therefore be used for the rectification of optical frequencies.[10,20] The efficiency of a rectification in the visible range has however still to be determined.

Previous theoretical work on these junctions has usually relied on approximations in the shape of the barrier and in the tunneling probabilities, which were typically based on a one-dimensional picture of the problem.[21] Modern computational facilities make it possible to address this problem using quantum-mechanical techniques that do not depend on these approximations but rather treat these aspects exactly by taking account of three-dimensional aspects of the problem. In a previous publication,[20] we presented a transfer-matrix analysis of this problem, which confirmed the conclusions achieved by Lucas *et al.*[18,19] and explored the dependence of the rectification properties of these systems on their physical and geometrical parameters. This analysis still relied on a quasistatic approximation, in which it is assumed that one can compare currents obtained for static values of the external bias. This approximation is valid in far infrared (frequency $\Omega \rightarrow 0$) but must be replaced by a more exact approach in order to treat situations, in which the time that electrons take to cross the junction is comparable with the period of the oscillating barrier.

This paper extends our previous work by taking into account the time dependence of the external bias explicitly. As in our previous work, we focus on a system that consists of a cathode with an hemispherical protrusion and a flat anode. The transfer-matrix methodology that we use for the electronic scattering calculations was adapted in order to account for the time dependence of the external bias. These methodological developments are presented in Sec. II. In Sec. III, we discuss numerical aspects of this methodology by considering first the case in which the junction is symmetric. We then address in Sec. IV the geometrically asymmetric junction already considered in our quasistatic analysis. We show that the results obtained in that previous analysis agree with those achieved in this oscillating-barrier analysis in the limit when $\Omega \rightarrow 0$. Extending our previous work, we then study in Sec. V the dependence of the rectification properties of this junction on the frequency and amplitude of the oscillating barrier. We also determine the power this device could provide to an external load and the efficiency with which the energy of an incident radiation could be converted into a

useful dc. The results presented in this paper demonstrate that the rectification of optical frequencies is possible using nanoscale devices of the type discussed here.

II. METHODOLOGY: TRANSFER-MATRIX THEORY FOR THE CALCULATION OF ELECTRONIC SCATTERING IN A JUNCTION SUBJECTED TO AN OSCILLATING POTENTIAL

The typical situation we consider is that where two tungsten metals, delimited by flat parallel surfaces, are separated by a distance D. The surface of these two metals are referred to by $z=0$ and D, where z is a vertical axis that is perpendicular to these surfaces. The intermediate region contains the potential-energy distributions that are responsible for the electronic scattering, which is in particular the hemispherical protrusion on the lower metal. We assume that the lower metal (region I) and the upper metal (region III) are perfect metals characterized by a Fermi energy E_F and a work function W (for tungsten, we take $E_F=19.1$ eV and $W=4.5$ eV). The intermediate region $0 \leq z \leq D$ is also referred to as region II.

We assume that the junction is subjected to an oscillating bias of the form $V_{ext}(t)=V_{ext}\cos(\Omega t)$, so that the potential energy takes the form[22]

$$V(\mathbf{r},t) = V_{stat}(\mathbf{r}) + V_{osc}(\mathbf{r})\cos(\Omega t). \tag{1}$$

In this expression, $V_{stat}(\mathbf{r})$ contains the image potential $E_{image}(\mathbf{r})$ that expresses the interaction of the tunneling electrons with the metallic elements[23] as well as the $-(E_F+W)$ potential wells that are representative of these metallic elements. $V_{osc}(\mathbf{r})$ describes the oscillating part of the potential energy and is only related to the external bias $V_{ext}(t)$. It is assumed by convention that $V_{stat}(\mathbf{r})=V_{I/III}=-(E_F+W)$ in regions I and III, while $V_{osc}(\mathbf{r})=0$ in region I and $V_{osc}(\mathbf{r})=V_{osc}=-eV_{ext}$ in region III, with e as the absolute value of the electronic charge. The values of $V_{stat}(\mathbf{r})$ and $V_{osc}(\mathbf{r})$ in the intermediate region II are calculated using the finite-difference techniques presented in Ref. 20 and 24. Figures 1 and 6 illustrate $V_{stat}(\mathbf{r})$ and $V_{osc}(\mathbf{r})$ in the intermediate region II for the geometrically symmetric and asymmetric junctions considered hereafter.

Using the transfer-matrix methodology developed in Refs. 25–30, one can then compute the currents that flow between the two metals. The idea consists in expressing the wave function $\Psi(\mathbf{r},t)$ that represents the electrons is provided by the bottom and the top metals by

$$\Psi(\mathbf{r},t) = \sum_{k=-N}^{N} \Psi_k(\mathbf{r}) e^{-i(E+k\hbar\Omega)t/\hbar}, \tag{2}$$

where N is a cutoff parameter for the number of quanta $\hbar\Omega$ the electrons represented by $\Psi(\mathbf{r},t)$ can absorb or emit because of their interaction with the oscillating barrier.[29–31] $\Psi_k(\mathbf{r})$ are actually the components of the wave function associated with the energy $E+k\hbar\Omega$. By injecting the expressions (1) and (2) in the time-dependent Schrödinger equation $[-\frac{\hbar^2}{2m}\Delta + V(\mathbf{r},t)]\Psi(\mathbf{r},t) = i\hbar\frac{\partial}{\partial t}\Psi(\mathbf{r},t)$, one obtains a system of coupled equations of the form

$$\left[-\frac{\hbar^2}{2m}\Delta + V_{stat}(\mathbf{r})\right]\Psi_k(\mathbf{r}) + \frac{1}{2}V_{osc}(\mathbf{r})[\Psi_{k-1}(\mathbf{r}) + \Psi_{k+1}(\mathbf{r})] = (E + k\hbar\Omega)\Psi_k(\mathbf{r}), \tag{3}$$

in which the amplitude $V_{osc}(\mathbf{r})$ of the oscillating part of the potential energy turns out to be responsible for the coupling between the components $\Psi_k(\mathbf{r})$ of the wave function.[29]

In order to introduce a quantification of the electronic states, we work in cylindrical coordinates and assume that the electrons are confined in a cylinder with radius R (we take as in our previous work $R=2$ nm). The boundary states in regions I and III are then given by[29]

$$\Psi^{I,\pm}_{m,j,k}(\mathbf{r},t) = \frac{RJ_m(k_{m,j}\rho)\exp(im\phi)}{\sqrt{2\int_0^R d\rho\rho[J_m(k_{m,j}\rho)]^2}} e^{\pm i\sqrt{(2m/\hbar^2)(E+k\hbar\Omega-V_I)-k_{m,j}^2 z}} e^{-i(E+k\hbar\Omega)t/\hbar}, \tag{4}$$

$$\Psi^{III,\pm}_{m,j,k}(\mathbf{r},t) = \frac{RJ_m(k_{m,j}\rho)\exp(im\phi)}{\sqrt{2\int_0^R d\rho\rho[J_m(k_{m,j}\rho)]^2}} e^{\pm i\sqrt{(2m/\hbar^2)(E+\lambda_k-V_{III})-k_{m,j}^2 z}} \sum_{k'=-N}^{N} V_{k',k} e^{-i(E+k'\hbar\Omega)t/\hbar}, \tag{5}$$

where J_m refer to Bessel functions and $k_{m,j}$ to the radial component of the wave vector. $k_{m,j}$ are defined by the conditions $J'_m(k_{m,j}R)=0$, where J'_m refer to the derivative of the Bessel functions and $\frac{\hbar^2 k_{m,j}^2}{2m} \leq E_{cutoff}$, with E_{cutoff} as a cutoff parameter used to limit the boundary states. Convergence is achieved by taking $E_{cutoff}=E+N\hbar\Omega+|V_{osc}|-V_{stat}^{min}+\Delta E$, where $V_{stat}^{min}=\min_{\mathbf{r}} V_{stat}(\mathbf{r})$ is the smallest value of the static part of the potential energy (as found on the grids that describe the whole system) and $\Delta E=2$ eV. The $\pm$ signs refer to the propagation direction relative to the z axis. λ_k and $V_{k',k}$ refer,

respectively, to the eigenvalues and components of the eigenvectors of the matrix

$$\mathbf{M} = \begin{pmatrix} N\hbar\Omega & -V_{\mathrm{osc}}/2 & & & \\ -V_{\mathrm{osc}}/2 & (N-1)\hbar\Omega & -V_{\mathrm{osc}}/2 & & \\ & \ddots & \ddots & \ddots & \\ & & -V_{\mathrm{osc}}/2 & -(N-1)\hbar\Omega & -V_{\mathrm{osc}}/2 \\ & & & -V_{\mathrm{osc}}/2 & -N\hbar\Omega \end{pmatrix}. \tag{6}$$

Since $V_{\mathrm{osc}}(\mathbf{r})=0$ in region I, the boundary states $\Psi^{\mathrm{I},\pm}_{m,j,k}(\mathbf{r},t)$ in the bottom metal turn out to have an energy given by $E(t)=E+k\hbar\Omega$. In region III, $V_{\mathrm{osc}}(\mathbf{r})=V_{\mathrm{osc}}$ is nonzero in general and the boundary states $\Psi^{\mathrm{III},\pm}_{m,j,k}(\mathbf{r},t)$ contain different energy components. In the limit when $N\to\infty$, the energy of these states is actually given by $E(t)=E+k\hbar\Omega+V_{\mathrm{osc}}\cos(\Omega t)$, so that the boundary states $\Psi^{\mathrm{I},\pm}_{m,j,k}$ and $\Psi^{\mathrm{III},\pm}_{m,j,k}$ can both be interpreted as resulting from the absorption or emission of k quanta of energy $\hbar\Omega$. In addition, the energy of the boundary states $\Psi^{\mathrm{III},\pm}_{m,j,k}$ turns out to follow the oscillations of the reference potential in that region. We demonstrate in Appendix A some important properties of the boundary states $\Psi^{\mathrm{III},\pm}_{m,j,k}$ in the anode region III.

Since the boundary states $\Psi^{\mathrm{I},\pm}_{m,j,k}$ and $\Psi^{\mathrm{III},\pm}_{m,j,k}$ have a well-defined physical meaning, one can use the techniques presented in Ref. 29 and build scattering solutions of the form

$$\begin{aligned} \Psi^{+}_{m,j,0} &\overset{\mathbf{r}\in\text{region I}}{=} \Psi^{\mathrm{I},+}_{m,j,0} + \sum_{m',j',k'} S^{-+}_{(m',j',k'),(m,j,0)} \Psi^{\mathrm{I},-}_{m',j',k'} \\ &\overset{\mathbf{r}\in\text{region III}}{=} \sum_{m',j',k'} S^{++}_{(m',j',k'),(m,j,0)} \Psi^{\mathrm{III},+}_{m',j',k'}, \end{aligned} \tag{7}$$

$$\begin{aligned} \Psi^{-}_{m,j,0} &\overset{\mathbf{r}\in\text{region I}}{=} \sum_{m',j',k'} S^{--}_{(m',j',k'),(m,j,0)} \Psi^{\mathrm{I},-}_{m',j',k'} \\ &\overset{\mathbf{r}\in\text{region III}}{=} \Psi^{\mathrm{III},-}_{m,j,0} + \sum_{m',j',k'} S^{+-}_{(m',j',k'),(m,j,0)} \Psi^{\mathrm{III},+}_{m',j',k'}, \end{aligned} \tag{8}$$

which correspond to single-incident states $\Psi^{\mathrm{I},+}_{m,j,0}$ and $\Psi^{\mathrm{III},-}_{m,j,0}$ in the bottom and top metals for a given value of the energy E. The $S^{++}_{(m',j',k'),(m,j,0)}$ and $S^{-+}_{(m',j',k'),(m,j,0)}$ factors provide, respectively, the coefficients of the transmitted and reflected states for each incident state $\Psi^{\mathrm{I},+}_{m,j,0}$ in the bottom metal. Similarly, the $S^{--}_{(m',j',k'),(m,j,0)}$ and $S^{+-}_{(m',j',k'),(m,j,0)}$ factors provide, respectively, the coefficients of the transmitted and reflected states for each incident state $\Psi^{\mathrm{III},-}_{m,j,0}$ in the top metal. The $\mathbf{S}^{\pm\pm}$ matrices that contain these coefficients satisfy unitary properties (when the potential energy is real valued and when the group velocities discussed hereafter are included in the normalization of the boundary states).[32–35] These properties express essentially the principle of charge conservation and the linear independence of the scattering solutions. The calculation of the $\mathbf{S}^{\pm\pm}$ matrices is actually more efficient when the techniques presented in Ref. 26–28 are used. The conductance of the system described by these matrices comes from the contribution of every channel associated with a couple of propagative states in both the regions of incidence and transmission. The conductance of each channel is merely proportional to the squared amplitude of the corresponding element in the $\mathbf{S}^{++}$ matrix for the upward current or in the $\mathbf{S}^{--}$ matrix for the downward current. The properties of the metal-vacuum-metal junctions considered in this paper could therefore be analyzed in terms of those of the scattering matrices.[35] We rather focused our discussion on the currents that cross the junction.

The currents that flow between the two metals hence result from the contribution of every solution associated with a propagative state in the region of incidence. The mean current that flows from the cathode region I to the anode region III is actually given by

$$\begin{aligned} \langle I^{+}\rangle = \frac{2e}{h}\int_{V_{\mathrm{I}}}^{+\infty} \sum_{m,j}\sum_{m',j',k'} & f_{\mathrm{I}}(E)[1-f_{\mathrm{III}}(\bar{E}^{\mathrm{III}}_{m,j,0})] \\ & \times \frac{v_{\mathrm{III},(m',j',k')}}{v_{\mathrm{I},(m,j,0)}} |S^{++}_{(m',j',k'),(m,j,0)}|^2 dE, \end{aligned} \tag{9}$$

while the mean current that flows from the anode region III to the cathode region I is given by

$$\begin{aligned} \langle I^{-}\rangle = \frac{2e}{h}\int_{V_{\mathrm{III}}}^{+\infty} \sum_{m,j}\sum_{m',j',k'} & f_{\mathrm{III}}(E)[1-f_{\mathrm{I}}(\bar{E}^{\mathrm{I}}_{m,j,0})] \\ & \times \frac{v_{\mathrm{I},(m',j',k')}}{v_{\mathrm{III},(m,j,0)}} |S^{--}_{(m',j',k'),(m,j,0)}|^2 dE, \end{aligned} \tag{10}$$

where we take the convention to give to both the upward and downward currents positive values. It is of course understood that the physical currents associated with $\langle I^{+}\rangle$ and $\langle I^{-}\rangle$ flow in opposite directions. In these expressions, $v_{\mathrm{I},(m,j,k)}=\frac{\hbar}{m}\sqrt{\frac{2m}{\hbar^2}(E+k\hbar\Omega-V_{\mathrm{I}})-k^2_{m,j}}$ and $v_{\mathrm{III},(m,j,k)}=\frac{\hbar}{m}\sqrt{\frac{2m}{\hbar^2}(E+\lambda_k-V_{\mathrm{III}})-k^2_{m,j}}$ refer to the group velocity in the bottom and top metals. $f_{\mathrm{I}}(E)=1/\{\exp[(E-\mu_{\mathrm{I}})/k_{\mathrm{B}}T]+1\}$ and $f_{\mathrm{III}}(E)=1/\{\exp[(E-\mu_{\mathrm{III}})/k_{\mathrm{B}}T]+1\}$ are the Fermi factors in either the top or the bottom metal, with $\mu_{\mathrm{I/III}}=-W$ as the chemical potential and $T=300$ K as the temperature of the two metals. k_{B} is the Boltzmann constant. $\bar{E}^{\mathrm{III}}_{m,j,0}$ and $\bar{E}^{\mathrm{I}}_{m,j,0}$ refer to the mean energy of the transmitted part of the wave functions. They are defined, respectively, by

$$\bar{E}^{\mathrm{III}}_{m,j,0} = \frac{\sum_{m',j',k'} |S^{++}_{(m',j',k'),(m,j,0)}|^2 (E + k'\hbar\Omega)}{\sum_{m',j',k'} |S^{++}_{(m',j',k'),(m,j,0)}|^2}, \quad (11)$$

$$\bar{E}^{\mathrm{I}}_{m,j,0} = \frac{\sum_{m',j',k'} |S^{--}_{(m',j',k'),(m,j,0)}|^2 (E + k'\hbar\Omega)}{\sum_{m',j',k'} |S^{--}_{(m',j',k'),(m,j,0)}|^2}. \quad (12)$$

The sums in expressions (9)–(12) must actually be restricted to propagative states.[33] The mean value of the net current that flows from the cathode region I to the anode region III is then given by $\langle I\rangle = \langle I^+\rangle - \langle I^-\rangle$. Since the external bias $V_{\mathrm{ext}}(t) = V_{\mathrm{ext}} \cos(\Omega t)$ is oscillating in time, the currents that flow between the two metals will actually also depend on time. We provide in Appendix B analytical expressions for the Fourier components I^+_k and I^-_k of the upward and downward currents, which enable the time dependence $I^+(t) = \Sigma_{k=-2N}^{2N} I^+_k e^{ik\Omega t}$ and $I^-(t) = \Sigma_{k=-2N}^{2N} I^-_k e^{ik\Omega t}$ of these currents to be calculated explicitly.

Another quantity of interest is the power gained by the electrons that cross the junction from the source of the oscillating barrier. With $I(t) = \Sigma_{k=-2N}^{2N} I_k e^{ik\Omega t}$ the net current that flows through the junction ($I_k = I^+_k - I^-_k$) and with $V_{\mathrm{ext}}(t) = V_{\mathrm{ext}} \frac{e^{i\Omega t} + e^{-i\Omega t}}{2}$ the bias applied to the junction, a classical way to compute the power gained from the source of the external bias would be

$$\langle P_{\mathrm{classic}}\rangle = \frac{1}{T}\int_0^T V_{\mathrm{ext}}(t) I(t) dt = \begin{cases} V_{\mathrm{ext}} I_0 & \text{if } \Omega = 0 \\ V_{\mathrm{ext}} \dfrac{I_1 + I_{-1}}{2} & \text{if } \Omega \neq 0 \end{cases}, \quad (13)$$

where $T = \frac{2\pi}{\Omega}$ is the period of the external bias. This definition makes sense only in conditions where the time taken by electrons to cross the device is much smaller than the period T of the external bias ($\Omega \to 0$). This is usually the case with frequencies in infrared.

In conditions where the time taken by electrons to cross the junction is comparable with the period of the external bias, one must actually compute the power gained from the source of the external bias by using the following quantum-mechanical expression:

$$\langle P_{\mathrm{quantum}}\rangle = \sum_{k=-N}^{N} k\hbar\Omega \langle I_k\rangle. \quad (14)$$

The factor $\langle I_k\rangle$ refers to the part of the mean current $\langle I\rangle$ that is due to the component $\Psi_k(\mathbf{r})$ of the wave functions,

$$\langle I_k\rangle = \frac{2e}{h}\int_{V_{\mathrm{I}}}^{+\infty} \sum_{m,j}\sum_{m',j'} f_{\mathrm{I}}(E)[1 - f_{\mathrm{III}}(\bar{E}^{\mathrm{III}}_{m,j,0})] \frac{v_{\mathrm{III},(m',j',k)}}{v_{\mathrm{I},(m,j,0)}} |S^{++}_{(m',j',k),(m,j,0)}|^2 dE$$
$$- \frac{2e}{h}\int_{V_{\mathrm{III}}}^{+\infty} \sum_{m,j}\sum_{m',j'} f_{\mathrm{III}}(E)[1 - f_{\mathrm{I}}(\bar{E}^{\mathrm{I}}_{m,j,0})] \frac{v_{\mathrm{I},(m',j',k)}}{v_{\mathrm{III},(m,j,0)}} |S^{--}_{(m',j',k),(m,j,0)}|^2 dE. \quad (15)$$

We will observe that $\langle P_{\mathrm{classic}}\rangle$ and $\langle P_{\mathrm{quantum}}\rangle$ provide similar values when Ω is small (typically in infrared), while only $\langle P_{\mathrm{quantum}}\rangle$ continues providing meaningful values when we get closer to the visible spectrum.

III. APPLICATION: ANALYSIS OF THE PROPERTIES OF A SYMMETRIC BARRIER SUBJECTED TO AN OSCILLATING POTENTIAL

In order to demonstrate the validity of this methodology and address some important numerical issues, we will first consider the case in which the barrier is symmetric. We expect of course the upward and downward currents to be symmetric except for a time shift corresponding to one half of the period of the external bias. We take the same conditions as in our quasistatic analysis,[20] i.e., a spacing D of 2 nm between the cathode and the anode and an amplitude V_{ext} of the external bias of 1 V. For these simulations, we give Ω the value that corresponds to a quantum of energy $\hbar\Omega$ of 0.5 eV. This corresponds to a radiation wavelength of 2480 nm in infrared. The static and oscillating parts of the potential barrier that correspond to this situation are depicted in Fig. 1.

The time dependence of the upward and downward currents $I^+(t)$ and $I^-(t)$ are represented in Fig. 2. It appears immediately that these currents are identical except for a time shift corresponding to one half of the period $T = 2\pi/\Omega$ of the oscillating barrier. The current emitted by the bottom metal is indeed expected to be maximal when the barrier is "down" ($t = i2\pi/\Omega$ with i as an integer), while the current emitted by the top metal is expected to be maximal when the barrier is "up" ($t = \pi/\Omega + i2\pi/\Omega$ with i as an integer). Because of the time that electrons take to cross this junction, there is actually a time shift Δt of $0.022(2\pi/\Omega)$ between the peak intensities of the oscillating barrier and those of the diode currents. The relative time shift $\Delta t/T$ turns out to increase with the frequency of the oscillating barrier. This can be understood if we consider that the time that electrons take to cross the junction contains a part that is intrinsic to the dynamics of these electrons, in particular to the tunneling process that

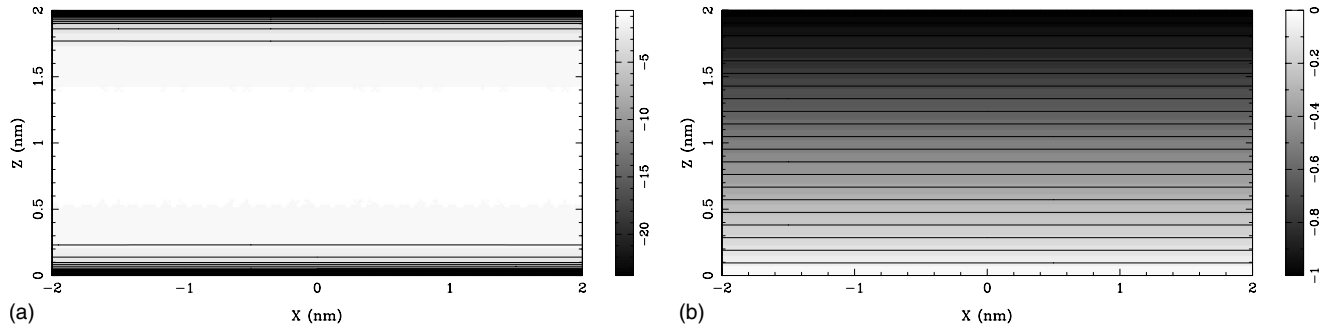

FIG. 1. Static part $V_{\mathrm{stat}}(\mathbf{r})$ (left) and oscillating part $V_{\mathrm{osc}}(\mathbf{r})$ (right) of the potential energy $V(\mathbf{r},t)=V_{\mathrm{stat}}(\mathbf{r})+V_{\mathrm{osc}}(\mathbf{r})\cos(\Omega t)$. $V_{\mathrm{stat}}(\mathbf{r})$ includes the image potential and the potential wells that characterize the metallic elements. $V_{\mathrm{osc}}(\mathbf{r})$ describes the effects of the $V_{\mathrm{ext}}(t)=V_{\mathrm{ext}}\cos(\Omega t)$ external bias, whose amplitude V_{ext} is 1 V.

takes place in the classically forbidden part of the potential barrier. A detailed analysis of these time shifts may thus lead to an estimation of this tunneling time.[10] This analysis was however left for future work. The results obtained in Sec. IV actually show that these time shifts are higher for a flat surface than for a tip. This may be due to the fact the distance the electrons have to cross in the junction is larger when the two electrodes are flat.

The Fourier components I_k^+ of the upward current $I^+(t)=\Sigma_{k=-2N}^{2N} I_k^+ e^{ik\Omega t}$ are represented in Fig. 3. The Fourier coefficients of the downward current are identical except for a phase factor due to the π/Ω time shift between the upward and downward currents $[I_k^-=(-1)^k I_k^+]$. The main quantity of interest in this figure is I_0^+, as it provides the mean value $\langle I^+\rangle=\frac{1}{T}\int_0^T I^+(t)dt$ of the upward current. We have in this case $\langle I^+\rangle=\langle I^-\rangle=3.227\times10^{-19}$ A. Another quantity of interest is $\mathrm{Re}(I_1^+)$ because this quantity is related to the classical expression of the power $\langle P_{\mathrm{classic}}^+\rangle=\frac{1}{T}\int_0^T V_{\mathrm{ext}}(t)I^+(t)dt$ gained by the upward current from the source of the oscillating barrier. We have indeed $\langle P_{\mathrm{classic}}^+\rangle=V_{\mathrm{ext}}\frac{I_1^+ + I_{-1}^+}{2}=V_{\mathrm{ext}}\frac{I_1^+ + I_1^{+*}}{2}=V_{\mathrm{ext}}\,\mathrm{Re}(I_1^+)$. For a symmetric barrier, the power gained from the downward current from the source of the oscillating barrier is given by $\langle P_{\mathrm{classic}}^-\rangle=\langle P_{\mathrm{classic}}^+\rangle$. The net power gained from the source of the oscillating barrier is therefore given by $\langle P_{\mathrm{classic}}\rangle=2\langle P_{\mathrm{classic}}^+\rangle=2V_{\mathrm{ext}}\,\mathrm{Re}(I_1^+)=5.309\times10^{-19}$ W. For comparison, the quantum-mechanical expression of this same quantity is given by $\langle P_{\mathrm{quantum}}\rangle=\Sigma_{k=-N}^{N}k\hbar\Omega\langle I_k\rangle=7.311\times10^{-19}$ W, where $\langle I_k\rangle$ is defined in Eq. (15). The classical expression $\langle P_{\mathrm{classic}}\rangle=\frac{1}{T}\int_0^T V_{\mathrm{ext}}(t)I(t)dt$ therefore underestimate by 27% the power gained from the source of the oscillating barrier. This discrepancy is due to the fact the external bias $V_{\mathrm{ext}}(t)$ changes by a non-negligible amount during the time that electrons take to cross the junction. We will compare $\langle P_{\mathrm{classic}}\rangle$ and $\langle P_{\mathrm{quantum}}\rangle$ more systematically with the geometrically asymmetric barrier considered in Sec. IV. The other Fourier components I_k^+ finally provide information on the capacity of this junction to generate harmonics of the frequency of the external bias.

The results presented in Figs. 2 and 3 were achieved by considering basis states $\Psi_{m,j,k}^{\mathrm{I},\pm}$ and $\Psi_{m,j,k}^{\mathrm{III},\pm}$ that correspond to $|m|\leq m_{\max}=10$ and $k\leq N=12$. To check that these cutoff parameters are appropriate, it is useful to represent the contribution of each value of m or k to the mean upward current $\langle I^+\rangle$. These contributions are defined by

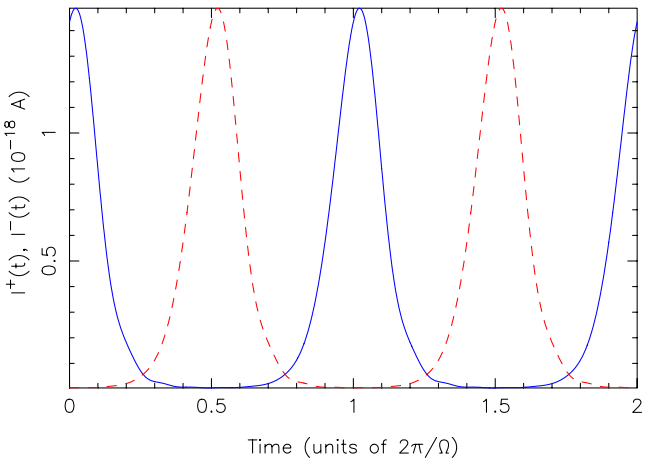

FIG. 2. (Color online) Time dependence of the upward (solid line) and downward (dashed line) currents as obtained for a symmetric barrier. The external bias $V_{\mathrm{ext}}(t)=V_{\mathrm{ext}}\cos(\Omega t)$ is characterized by an amplitude V_{ext} of 1 V and a pulsation Ω that corresponds to a quantum of energy $\hbar\Omega$ of 0.5 eV.

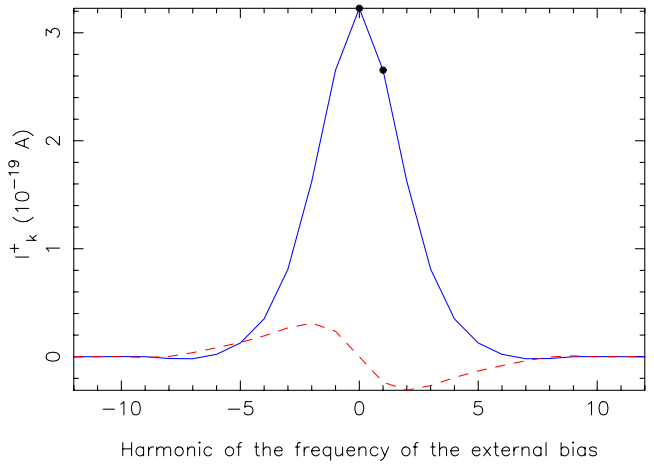

FIG. 3. (Color online) Fourier components of the upward current. The solid line stands for the real part and the dashed line for the imaginary part. The barrier is symmetric. The external bias $V_{\mathrm{ext}}(t)=V_{\mathrm{ext}}\cos(\Omega t)$ is characterized by an amplitude V_{ext} of 1 V and a pulsation Ω that corresponds to a quantum of energy $\hbar\Omega$ of 0.5 eV.

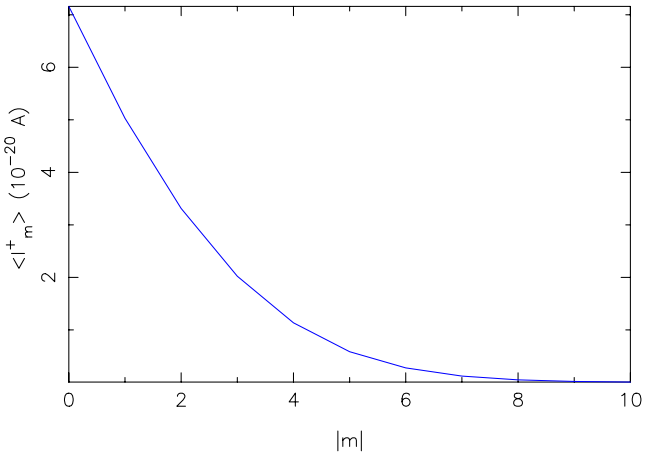

FIG. 4. (Color online) Contribution $\langle I_m^+ \rangle$ of each value of m to the mean value of the upward current. The barrier is symmetric. The external bias $V_{\text{ext}}(t)=V_{\text{ext}}\cos(\Omega t)$ is characterized by an amplitude V_{ext} of 1 V and a pulsation Ω that corresponds to a quantum of energy $\hbar\Omega$ of 0.5 eV.

$$\langle I_{\bar{m}}^+ \rangle = \frac{2e}{h}\int_{V_{\text{I}}}^{+\infty} \sum_{m,j} \sum_{j',k'} f_{\text{I}}(E)[1 - f_{\text{III}}(\bar{E}^{\text{III}}_{m,j,0})] \times \frac{v_{\text{III},(\bar{m},j',k')}}{v_{\text{I},(m,j,0)}} |S^{++}_{(\bar{m},j',k'),(m,j,0)}|^2 dE, \tag{16}$$

$$\langle I_{\bar{k}}^+ \rangle = \frac{2e}{h}\int_{V_{\text{I}}}^{+\infty} \sum_{m,j} \sum_{m',j'} f_{\text{I}}(E)[1 - f_{\text{III}}(\bar{E}^{\text{III}}_{m,j,0})] \times \frac{v_{\text{III},(m',j',\bar{k})}}{v_{\text{I},(m,j,0)}} |S^{++}_{(m',j',\bar{k}),(m,j,0)}|^2 dE, \tag{17}$$

and represented in Figs. 4 and 5.

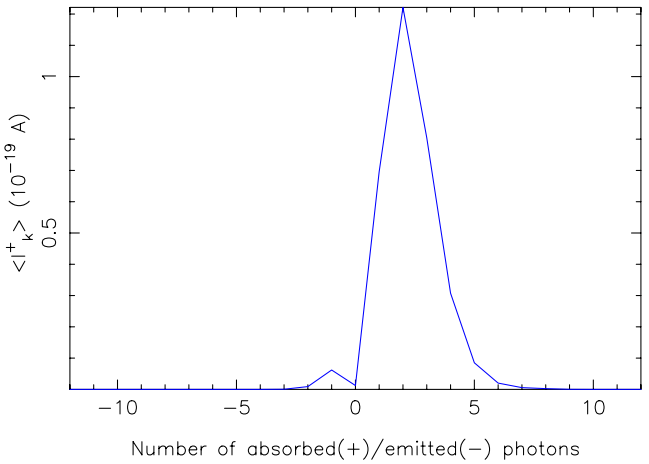

FIG. 5. (Color online) Contribution $\langle I_k^+ \rangle$ of each value of k to the mean value of the upward current. The barrier is symmetric. The external bias $V_{\text{ext}}(t)=V_{\text{ext}}\cos(\Omega t)$ is characterized by an amplitude V_{ext} of 1 V and a pulsation Ω that corresponds to a quantum of energy $\hbar\Omega$ of 0.5 eV.

Figure 4 confirms that it is necessary to take $m_{\max}=10$ in order to compute the upward and downward currents when the barrier is symmetric. In Sec. IV, we will extend the cathode by an hemispherical protrusion. For this same photon energy of 0.5 eV, the cutoff parameter $m_{\max}$ could be reduced to a value of 3. The tip has indeed a filtering effect, which gives the basis states associated with small values for m a higher probability to cross the surface barrier (the Bessel functions J_m that define these basis states have indeed more pronounced values around the central z axis when m is small). The calculations presented in this paper were however achieved by letting m go as high as necessary in order to reach convergence.

Figure 5 shows that the cutoff parameter N must be at least as large as 8 as $\langle I_k^+ \rangle$ takes significant values up to $k=8$. According to the material presented in Appendix A, the cutoff parameter N must actually be still larger in order for the representation of the boundary states in region III to be appropriate. The calculations presented in this section were actually achieved by taking $N=12$ and this parameter was adapted automatically in the remaining part of this paper according to the convergence criteria presented in Appendix A. Besides these convergence aspects, Fig. 5 also shows that the main contribution to the upward current is provided by electrons that have absorbed two quanta of energy $\hbar\Omega$. This can be understood by the fact that these quanta have an energy of 0.5 eV, while the amplitude of the oscillating barrier is 1 eV. The current emitted by the bottom metal is indeed maximal when the barrier is down (electric field oriented to the bottom metal). Since $V_{\text{osc}}=-1$ eV, the Fermi level of the bottom metal is then 1 eV above that of the anode metal. Physically, one can therefore expect the electrons emitted from the cathode metal to enter the anode metal with an energy higher by 1 eV than the Fermi level of the anode metal. In our formulation of this scattering problem, this is only possible if the electrons have absorbed two quanta $\hbar\Omega$. In conditions in which $|V_{\text{osc}}| \ll \hbar\Omega$, one can expect the main contribution to the upward current to come from states with $k=0$. The contribution from states associated with $k=1$ will be smaller and proportional to the power-flux density of the incident radiation, while multiphoton-absorption processes will in general be negligible.

IV. APPLICATION: RECTIFICATION PROPERTIES OF A GEOMETRICALLY ASYMMETRIC JUNCTION SUBJECTED TO AN OSCILLATING POTENTIAL

Section III aimed at validating the methodology and at setting some important numerical issues. We consider now that the cathode metal supports a hemispherical protrusion with a height of 1 nm and a radius of 0.5 nm. We consider as in Sec. III that the amplitude V_{ext} of the external bias is 1 V. The conditions are therefore the same as in our quasistatic analysis[20] except for the fact the external bias is oscillating as $V_{\text{ext}}\cos(\Omega t)$ instead of keeping either the $+V_{\text{ext}}$ or $-V_{\text{ext}}$ static value. We actually expect the conclusions obtained in our quasistatic analysis to reach those corresponding to this oscillating-barrier analysis in the limit when $\Omega \to 0$.

We consider as in Sec. III that the external bias $V_{\text{ext}}(t)=V_{\text{ext}}\cos(\Omega t)$ is oscillating with a pulsation Ω that corre-

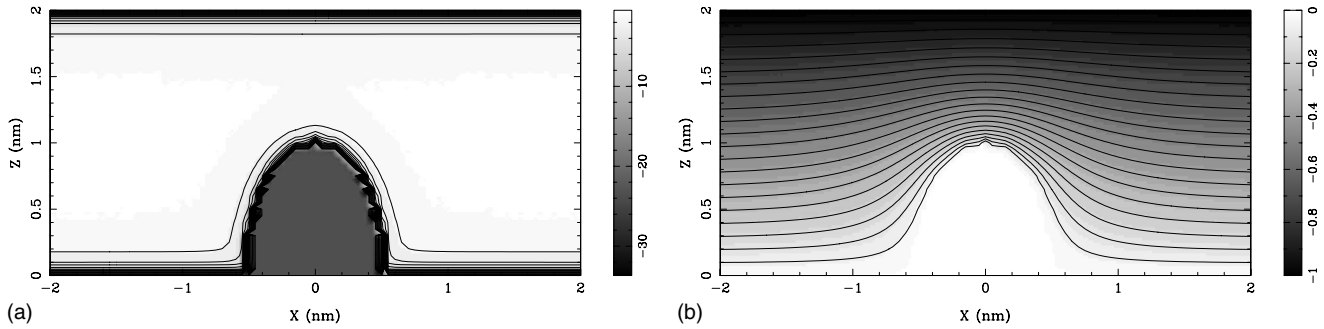

FIG. 6. Static part $V_{stat}(\mathbf{r})$ (left) and oscillating part $V_{osc}(\mathbf{r})$ (right) of the potential energy $V(\mathbf{r},t)=V_{stat}(\mathbf{r})+V_{osc}(\mathbf{r})\cos(\Omega t)$. $V_{stat}(\mathbf{r})$ includes the image potential and the potential wells that characterize the metallic elements. $V_{osc}(\mathbf{r})$ describes the effects of the $V_{ext}(t)=V_{ext}\cos(\Omega t)$ external bias, whose amplitude V_{ext} is 1 V.

sponds to an energy quantum $\hbar\Omega$ of 0.5 eV (radiation wavelength of 2480 nm in infrared). The static and oscillating parts of the potential energy are represented in Fig. 6. The image potential that applies to the electrons that cross the junction and the $-(E_F+W)$ potential wells that represent the metallic elements are included in the static part $V_{stat}(\mathbf{r})$ of the potential energy. The oscillating part $V_{osc}(\mathbf{r})$ of this potential energy accounts for the external bias.

The time dependence of the upward and downward currents is represented in Fig. 7. It appears very clearly that the magnitude of the upward current is larger than that of the downward current, which confirms dramatically the rectification properties of this junction. This rectification is solely due to the geometric asymmetry of the junction. The amplitude of the upward current is 2.567×10^{-12} A while that of the downward current is 1.174×10^{-12} A. These values are very close to the values of 2.476×10^{-12} and 1.421×10^{-12} A established in our quasistatic analysis.[20]

In order to compare these results with those obtained in Sec. III, we represented in Fig. 8 the Fourier components of the upward current. The distribution is actually sharper than for the symmetric barrier. One can establish that the mean values of the upward and downward currents are given, respectively, by $\langle I^+\rangle=8.501\times10^{-13}$ A and $\langle I^-\rangle=5.176\times10^{-13}$ A. The mean value of the net current that flows through the junction is hence given by $\langle I^+\rangle-\langle I^-\rangle=3.324\times10^{-13}$ A. If we define the rectification ratio of the junction by $R=\langle I^+\rangle/\langle I^-\rangle$, we get a value of 1.642, which is again very close to the value of 1.742 established in our quasistatic analysis.[20]

We hence obtain results that match reasonably well conclusions achieved in our quasistatic analysis of this problem. Differences are attributed to the fact the external bias oscillates as $V_{ext}(t)=V_{ext}\cos(\Omega t)$ in this analysis, while in our quasistatic analysis it was assumed implicitly that the external potential $V_{ext}(t)$ varies as a step function between $+V_{ext}$ and $-V_{ext}$. In this oscillating-barrier analysis, we take also into account of the fact that the electrons can absorb quanta of energy $\hbar\Omega$. This increases their probability to cross the surface barrier. These photon-absorption processes were not taken into account in the quasistatic analysis. These calculations provide therefore a further confirmation for the validity of this methodology and one can proceed with the analysis of this device.

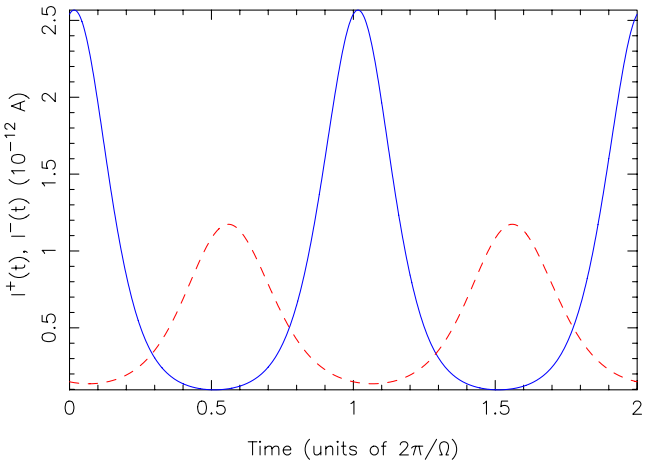

FIG. 7. (Color online) Time dependence of the upward (solid line) and downward (dashed line) currents as obtained for a geometrically asymmetric junction. The external bias $V_{ext}(t)=V_{ext}\cos(\Omega t)$ is characterized by an amplitude V_{ext} of 1 V and a pulsation Ω that corresponds to a quantum of energy $\hbar\Omega$ of 0.5 eV.

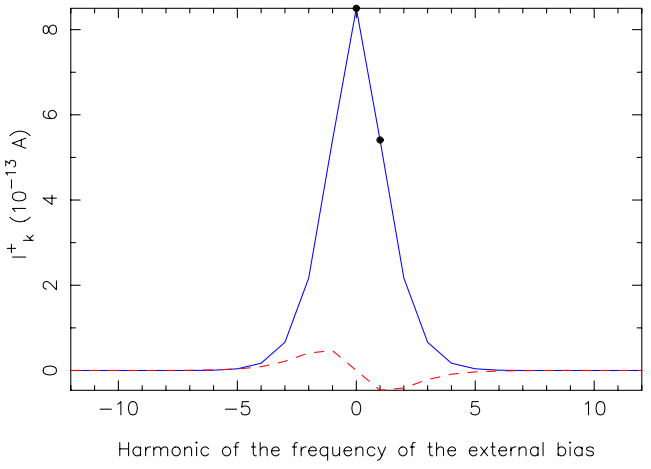

FIG. 8. (Color online) Fourier components of the upward current as obtained for a geometrically asymmetric junction. The solid line stands for the real part and the dashed line for the imaginary part. The external bias $V_{ext}(t)=V_{ext}\cos(\Omega t)$ is characterized by an amplitude V_{ext} of 1 V and a pulsation Ω that corresponds to a quantum of energy $\hbar\Omega$ of 0.5 eV.

For instance, the power $\langle P \rangle$ gained by the electrons that cross the junction from the source of the external bias is given by $\langle P_{\text{classic}} \rangle = 7.678 \times 10^{-13}$ W if one uses the classical expression given in Eq. (13). The quantum-mechanical evaluation of this same quantity provides a value of $\langle P_{\text{quantum}} \rangle = 8.707 \times 10^{-13}$ W. The classical expression $\langle P_{\text{classic}} \rangle = \frac{1}{T}\int_0^T V_{\text{ext}}(t) I(t) dt$ therefore underestimates by 11.8% the power gained by the electrons that cross the junction. This discrepancy is smaller than for the symmetric barrier. This may come from the fact that electrons take less time to cross the junction (the distance these electrons have to cross is indeed shorter and the fields at the apex of the protrusion are stronger). This reduction in the time that electrons take to cross the junction improves the applicability of the classical formula.

In a practical device, the oscillating barrier would result from a radiation incident on the junction (in this model we assume that an external battery is responsible for the polarization of the junction). In this context, we would define the input power on the tip as the power-flux density of the radiation times the area intercepted by the tip. In the conditions of this model and assuming that the field of the incident radiation can be estimated by $-V_{\text{ext}}/D$, the input power is given by $\langle P_{\text{in}} \rangle = \frac{\epsilon_0 c}{2}\left(\frac{V_{\text{ext}}}{D}\right)^2 \times \frac{\pi h_{\text{tip}} r_{\text{tip}}}{2} = 2.6 \times 10^{-4}$ W (r_{tip} and h_{tip} stand for the radius and height of the tip, respectively). The problem of calculating the coupling between an incident radiation and a junction whose characteristic size should be micrometers rather than nanometers goes beyond the scope of this paper and is left for future work. The nanometric dimensions of these simulations are dictated by the computational requirements of our methodology. An analysis of the coupling of an incident radiation with a microscopic tip can be found in the paper by Sullivan *et al.*[36]

V. SYSTEMATIC STUDY OF THE RECTIFICATION PROPERTIES OF GEOMETRICALLY ASYMMETRIC JUNCTIONS SUBJECTED TO AN OSCILLATING POTENTIAL

We keep the geometrically asymmetric junction of Sec. IV but consider now variations in either the amplitude or the frequency of the external bias $V_{\text{ext}}(t) = V_{\text{ext}} \cos(\Omega t)$. We keep for the moment an amplitude V_{ext} of 1 V and consider different values for the pulsation Ω, in particular the values that correspond to quanta of energy $\hbar\Omega$ ranging between 0.2 (radiation wavelength of 6200 nm in infrared) and 5 eV (radiation wavelength of 248 nm in ultraviolet).

The mean values $\langle I^+ \rangle$ and $\langle I^- \rangle$ that one obtains for the upward and downward currents, when $\hbar\Omega$ ranges between 0.2 and 5 eV, are represented in Fig. 9. The mean upward current turns out to be always higher than the mean downward current, which proves that the geometrically asymmetric junction depicted in Fig. 6 acts as a rectifier over this whole range of frequencies. The vertical lines indicate the height of the surface barrier when $V_{\text{ext}}(t)$ takes the values of 1, 0, and −1 V. This height is measured from the Fermi level of the metal that emits, i.e., the cathode when $V_{\text{ext}}(t) > 0$ and the anode when $V_{\text{ext}}(t) < 0$. These values indicate which quantum of energy $\hbar\Omega$ an electron at the Fermi level of either the bottom or the top metal has to absorb in order to cross the surface barrier by ballistic motion (in contrast to an emission by tunneling). Since the barrier is changing by the time that electrons cross the barrier, these values only serve as references. They explain however why $\langle I^+ \rangle$ and $\langle I^- \rangle$ increase more significantly when $\hbar\Omega > 3.65$ eV [the height of the surface barrier when $V_{\text{ext}}(t) = 0$].

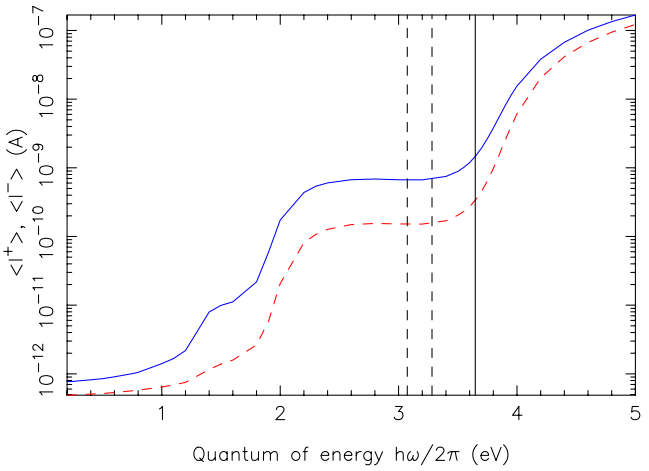

FIG. 9. (Color online) Mean value of the upward (solid line) and downward (dashed line) currents as obtained for a geometrically asymmetric junction subject to an external bias $V_{\text{ext}}(t) = V_{\text{ext}} \cos(\Omega t)$ with $V_{\text{ext}} = 1$ V and $\hbar\Omega$ ranging between 0.2 and 5 eV. The vertical lines indicate the height of the surface barrier (as measured from the Fermi level of the emitting metal) when $V_{\text{ext}}(t) = 1$ V (dashed line, left), $V_{\text{ext}}(t) = -1$ V (dashed line, right), and $V_{\text{ext}}(t) = 0$ V (solid line).

The rectification ratio $R = \langle I^+ \rangle / \langle I^- \rangle$ that one obtains by taking the ratio between the mean values of the upward and downward currents is represented in Fig. 10. The values obtained at low frequency ($\Omega \to 0$) agree with those obtained in our quasistatic analysis.[20] Because of the photon-absorption processes, the rectification ratio R first increases with Ω before decreasing at higher frequencies. The intermediate region proves that the rectification of optical frequencies can be achieved by the device depicted in Fig. 6, which agrees with early conclusions reached by Sullivan *et al.*[10] In our quasistatic analysis, we predicted a cutoff of the rectification for a photon energy $\hbar\Omega$ around 4 eV (radiation wavelength of 300 nm in ultraviolet) because it was estimated that the field would then reverse before the electrons can cross the junction. This oscillating-barrier analysis shows indeed a significant decrease in the rectification at that frequency.

We finally present in Fig. 11 the power gained by the electrons that cross the junction from the source of the oscillating barrier. These values are calculated from the quantum-mechanical expression provided in Eq. (14). These $\langle P_{\text{quantum}} \rangle$ values are compared with the classical expression $\langle P_{\text{classic}} \rangle = \frac{1}{T}\int_0^T V_{\text{ext}}(t) I(t) dt$, at least as long as this classical expression continues providing meaningful values. This already stops being the case for $\hbar\Omega = 1.5$ eV, as $\langle P_{\text{classic}} \rangle$ provides then negative values. The quantum-mechanical expression $\langle P_{\text{quantum}} \rangle$ on the other hand provides meaningful values on the full range of frequencies. These values follow essentially the variations in the mean upward current.

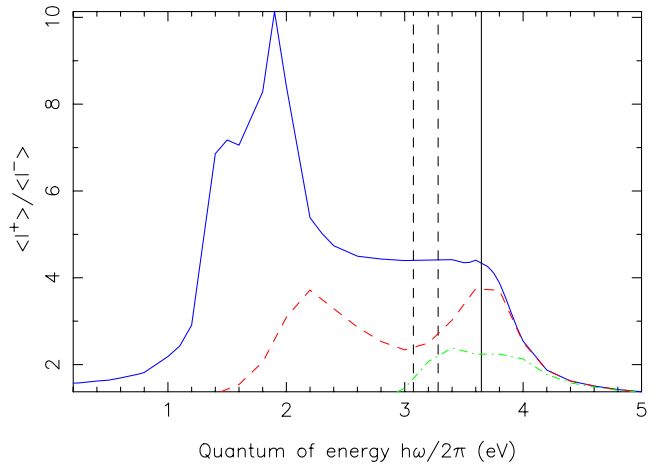

FIG. 10. (Color online) Rectification ratio as obtained for a geometrically asymmetric junction subject to an external bias $V_{ext}(t) = V_{ext} \cos(\Omega t)$ with $V_{ext}=1$ (solid line), 0.1 (dashed), and 0.01 V (dot-dashed line). The quantum of energy $\hbar\Omega$ ranges between 0.2 and 5 eV. The vertical lines indicate the height of the surface barrier (as measured from the Fermi level of the emitting metal) when $V_{ext}(t)=1$ (dashed line, left), −1 (dashed line, right), and 0 V (solid line).

This study of the rectification properties of geometrically asymmetric metal-vacuum-metal junctions focused on the frequency dependence of the currents that cross the junction. In order to distinguish between the effects that are due to the dynamics of the electrons and those that are due to the response of the material, we assumed that the cathode and the anode were perfect metals characterized by a given set of parameters, so that their answer to the oscillating field would be identical on the whole range of frequencies. In this study, photon-absorption processes turned out to have an important role for explaining the frequency dependence of the upward and downward currents. Since the efficiency of this photon-absorption process is proportional to the square of the oscillating field (i.e., $|V_{ext}/D|^2$), other factors become important when smaller values of V_{ext} are considered (in particular the time that electrons take to cross the junction). To illustrate the effects of a reduction in V_{ext}, we included in Figs. 10 and 11 the results that correspond to $V_{ext}=0.1$ and 0.01 V. The results actually show that $\langle P \rangle$ is essentially proportional to $(\frac{V_{ext}}{D})^2$ when $V_{ext} \leq 0.01$ V, while nonlinear effects associated with multiphoton-absorption processes play a significant role for higher values of V_{ext}. The objective of this paper was essentially to validate the methodology and extend the results of our quasistatic analysis. Future work will focus on physical parameters that were not included in this analysis.

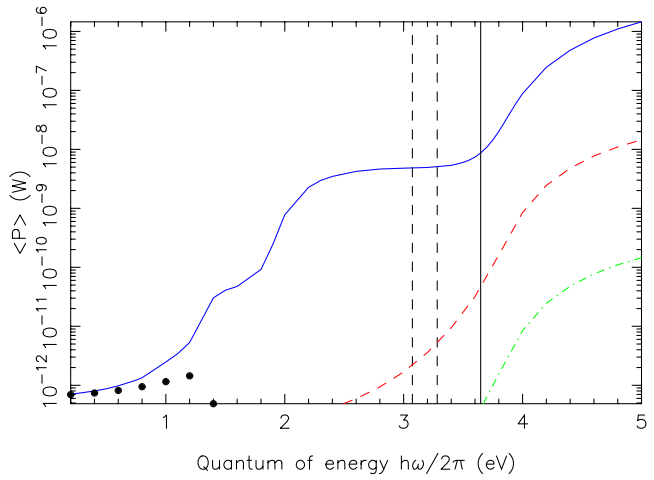

FIG. 11. (Color online) Power gained by the electrons that cross the junction from the source of the oscillating barrier as calculated from the quantum-mechanical expression $\langle P_{quantum} \rangle$. The dots indicate values calculated from the classical expression $\langle P_{classic} \rangle$. The junction is geometrically asymmetric and subjected to an external bias $V_{ext}(t) = V_{ext} \cos(\Omega t)$ with $V_{ext}=1$ (solid line), 0.1 (dashed line), and 0.01 V (dot-dashed line). The quantum of energy $\hbar\Omega$ ranges between 0.2 and 5 eV. The vertical lines indicate the height of the surface barrier (as measured from the Fermi level of the emitting metal) when $V_{ext}(t)=1$ (dashed line, left), −1 (dashed line, right), and 0 V (solid line).

VI. CONCLUSION

This paper proposed a quantum-mechanical approach to the rectification properties of geometrically asymmetric metal-vacuum-metal junctions treated as an oscillating barrier. This work is actually a generalization of our previous analysis, which was based on a quasistatic approximation. The methodology used to address this problem is the transfer-matrix technique, which enables the calculation of electronic scattering in metal-vacuum-metal junctions by taking into account three-dimensional aspects of the potential-energy distributions. This methodology was generalized in order to address the case in which the external bias is oscillating rather than just being constant. We proposed a detailed justification of this methodology and developed the main issues that arise in a numerical implementation. The validity of this methodology was demonstrated by considering first the case in which the junction is symmetric. We then addressed the geometrically asymmetric junction already considered in our quasistatic analysis. The results obtained at low frequency agree with those obtained in this previous work, which provides a further confirmation for the validity of this methodology. Extending our previous work, we then addressed the frequency dependence of the rectification properties of these junctions. In particular, we demonstrated the ability of nanometer-sized metal-vacuum-metal junctions to rectify optical frequencies. This extended analysis takes into account the photon-absorption processes that occur in the junction. It was demonstrated that these photon-absorption processes as well as the time that electrons take to cross the junction are important issues for the understanding of this device.

ACKNOWLEDGMENTS

A.M. is funded by the National Fund for Scientific Research (FNRS) of Belgium. The authors acknowledge the use of the Inter-university Scientific Computing Facility (ISCF) of Namur. A. A. Lucas and J. -P. Vigneron are acknowledged for their interest in this problem.

APPENDIX A: PROPERTIES OF THE EIGENSTATES OF SCHRÖDINGER'S EQUATION IN A REGION IN WHICH THE REFERENCE POTENTIAL IS OSCILLATING

We focus in this appendix on some fundamental properties of the eigenstates of Schrödinger's equation in a region in which the reference potential is oscillating in time (with otherwise a constant amplitude in space). This is the case of the anode region III, in which the reference potential oscillates as $V(\mathbf{r},t)=V_{\text{stat}}+V_{\text{osc}}\cos(\Omega t)$ with $V_{\text{stat}}=V_{\text{III}}$ standing for the steady part of the potential energy and V_{osc} for the amplitude of the oscillating part. Physically, one expects the term $V_{\text{osc}}\cos(\Omega t)$ to also appear in the energy of the eigenstates of this region and we will show that it is indeed the case.

The wave function can be expanded as $\Psi(\mathbf{r},t)=\sum_{k=-N}^{N}\Psi_k(\mathbf{r})e^{-i(E+k\hbar\Omega)t/\hbar}$, where N is a cutoff parameter discussed hereafter. We work in cylindrical coordinates and assume that the electrons are confined in a cylinder with radius R centered around the z axis. According to our previous work[29] and to Sec. II of this paper, the eigenstates of the time-dependent Schrödinger's equation $[-\frac{\hbar^2}{2m}\Delta+V(\mathbf{r},t)]\Psi(\mathbf{r},t)=i\hbar\frac{\partial}{\partial t}\Psi(\mathbf{r},t)$ are given by

$$\Psi_{m,j,k}^{\text{III},\pm}(\mathbf{r},t)=\frac{RJ_m(k_{m,j}\rho)\exp(im\phi)}{\sqrt{2\int_0^R d\rho\rho[J_m(k_{m,j}\rho)]^2}}e^{\pm i\sqrt{(2m/\hbar^2)(E+\lambda_k-V_{\text{stat}})-k_{m,j}^2}z}\sum_{k'=-N}^{N}V_{k',k}e^{-i(E+k'\hbar\Omega)t/\hbar} \tag{A1}$$

with J_m as the Bessel functions, $k_{m,j}$ as the radial component of the wave vector, and λ_k and $V_{k',k}$ as the eigenvalues and components of the eigenvectors of the matrix

$$\mathbf{M}=\begin{pmatrix} N\hbar\Omega & -V_{\text{osc}}/2 & & & \\ -V_{\text{osc}}/2 & (N-1)\hbar\Omega & -V_{\text{osc}}/2 & & \\ & \ddots & \ddots & \ddots & \\ & & -V_{\text{osc}}/2 & -(N-1)\hbar\Omega & -V_{\text{osc}}/2 \\ & & & -V_{\text{osc}}/2 & -N\hbar\Omega \end{pmatrix}. \tag{A2}$$

In the limit when $N\to\infty$, the eigenstates $\Psi_{m,j,k}^{\text{III},\pm}(\mathbf{r},t)$ take actually the form

$$\Psi_{m,j,k}^{\text{III},\pm}(\mathbf{r},t)\overset{N\to\infty}{=}\frac{RJ_m(k_{m,j}\rho)\exp(im\phi)}{\sqrt{2\int_0^R d\rho\rho[J_m(k_{m,j}\rho)]^2}}e^{\pm i\sqrt{(2m/\hbar^2)(E+k\hbar\Omega-V_{\text{stat}})-k_{m,j}^2}z}e^{-i(E+k\hbar\Omega)t/\hbar}e^{-i(V_{\text{osc}}/\hbar\Omega)\sin(\Omega t)}. \tag{A3}$$

The proof is obtained by defining $W_k(t)=\sum_{k'=-\infty}^{\infty}V_{k',k}e^{-ik'\Omega t}$. From the eigenvalue equation for λ_k, we have $k'\hbar\Omega V_{k',k}-\frac{V_{\text{osc}}}{2}(V_{k'-1,k}+V_{k'+1,k})=\lambda_k V_{k',k}$ and one can show that $W_k(t)$ satisfy the relation $i\hbar\frac{dW_k(t)}{dt}=[\lambda_k+V_{\text{osc}}\cos(\Omega t)]W_k(t)$. It follows that $W_k(t)=e^{(-i/\hbar)\int^t[\lambda_k+V_{\text{osc}}\cos(\Omega t')]dt'}=e^{(-i/\hbar)\{\lambda_k t+V_{\text{osc}}[\sin(\Omega t)/\Omega]\}}$. Periodicity in time enforces $\lambda_k=k\hbar\Omega$ and it is then easy to show that the energy of the eigenstates $\Psi_{m,j,k}^{\text{III},\pm}(\mathbf{r},t)$ is given by $E(t)\overset{N\to\infty}{=}E+k\hbar\Omega+V_{\text{osc}}\cos(\Omega t)$. This confirms that the eigenstates $\Psi_{m,j,k}^{\text{III},\pm}(\mathbf{r},t)$ can be interpreted as resulting from the absorption of k quanta of energy $\hbar\Omega$ and that their energy follows the oscillations of the reference potential. From the relation $W_k(t)=\sum_{k'=-\infty}^{\infty}V_{k',k}e^{-ik'\Omega t}=e^{-i[k\Omega t+(V_{\text{osc}}/\hbar\Omega)\sin(\Omega t)]}$, one can also show that $V_{k',k}\overset{N\to\infty}{=}\frac{\Omega}{2\pi}\int_0^{2\pi/\Omega}e^{i(k'-k)\Omega t}e^{-i(V_{\text{osc}}/\hbar\Omega)\sin(\Omega t)}dt$. It follows from this relation that $\sum_{k'=-\infty}^{\infty}V_{k'+i,k}^{*}V_{k',k}=\delta_{i,0}$, which will be useful for the following.

In any numeric calculation, N takes a finite value and it is essential to check that the boundary states $\Psi_{m,j,k}^{\text{III},\pm}(\mathbf{r},t)$ still provide a good approximation of the exact solutions. One can check that these states are orthonormalized and that their mean energy is given by

$$\begin{aligned}\frac{\langle\Psi_{m,j,k}^{\text{III},\pm}|H|\Psi_{m,j,k}^{\text{III},\pm}\rangle}{\langle\Psi_{m,j,k}^{\text{III},\pm}|\Psi_{m,j,k}^{\text{III},\pm}\rangle}&=\frac{\Omega}{2\pi}\int_0^{2\pi/\Omega}\sum_{k'=-N}^{N}V_{k',k}^{*}e^{i(E+k'\hbar\Omega)t/\hbar}\\&\quad\times\sum_{k''=-N}^{N}V_{k'',k}(E+k''\hbar\Omega)e^{-i(E+k''\hbar\Omega)t/\hbar}dt\\&=\sum_{k'=-N}^{N}(E+k'\hbar\Omega)|V_{k',k}|^2.\end{aligned} \tag{A4}$$

The time dependence of their energy can actually be calculated by

TABLE I. Numerical values of the eigenvalues λ_k and of the mean energies $\Sigma_{k'=-N}^{N} k'\hbar\Omega|V_{k',k}|^2$ as obtained in a simulation with $V_{\rm osc}=-1$ eV, $\hbar\Omega=0.5$ eV, and $N=12$. These values are compared with the limit $k\hbar\Omega$ that one obtains when $N\to\infty$.

k	λ_k	$\Sigma_{k'=-N}^{N} k'\hbar\Omega\|V_{k',k}\|^2$	$k\hbar\Omega$
−5	−2.500 000 001 904 06	−2.499 999 972 424 76	−2.5
−4	−2.000 000 000 027 24	−1.999 999 999 549 29	−2.0
−3	−1.500 000 000 000 31	−1.499 999 999 994 24	−1.5
−2	−1.000 000 000 000 00	−0.999 999 999 999 943	−1.0
−1	−0.500 000 000 000 000	−0.499 999 999 999 998	−0.5
0	$-2.256\,362\,437\,690\,874\times10^{-16}$	$-1.202\,993\,726\,273\,960\times10^{-15}$	0.0
1	0.500 000 000 000 000	0.499 999 999 999 999	0.5
2	1.000 000 000 000 00	0.999 999 999 999 943	1.0
3	1.500 000 000 000 31	1.499 999 999 994 24	1.5
4	2.000 000 000 027 24	1.999 999 999 549 29	2.0
5	2.500 000 001 904 07	2.499 999 972 424 76	2.5

$$
\begin{aligned}
E(t) &= \frac{1}{\pi R^2}\int_0^R d\rho\rho\int_0^{2\pi} d\phi\, \Psi_{m,j,k}^{\mathrm{III},\pm}(\mathbf{r},t)^* \\
&\times\left[-\frac{\hbar^2}{2m}\Delta + V_{\rm stat} + V_{\rm osc}\frac{e^{i\Omega t}+e^{-i\Omega t}}{2}\right]\Psi_{m,j,k}^{\mathrm{III},\pm}(\mathbf{r},t) \\
&= (E+\lambda_k)\sum_{k',k''} V_{k',k}^* V_{k'',k} e^{i(k'-k'')\Omega t} \\
&+ \frac{V_{\rm osc}}{2}\sum_{k',k''} V_{k',k}^* V_{k'',k}\left[e^{i(k'-k''+1)\Omega t} + e^{i(k'-k''-1)\Omega t}\right] \\
&= E_0 + 2\sum_{i=1}^{2N+1} E_i\cos(i\Omega t), \qquad \text{(A5)}
\end{aligned}
$$

where

$$
\begin{aligned}
E_i &= (E+\lambda_k)\sum_{k',k''} V_{k',k}^* V_{k'',k}\delta_{k',k''+i} \\
&+ \frac{V_{\rm osc}}{2}\sum_{k',k''} V_{k',k}^* V_{k'',k}\left[\delta_{k',k''+i-1} + \delta_{k',k''+i+1}\right]. \qquad \text{(A6)}
\end{aligned}
$$

In the limit where $N\to\infty$, we have $\lambda_k\to k\hbar\Omega$. The relation $\Sigma_{k'=-\infty}^{\infty} V_{k'+i,k}^* V_{k',k} = \delta_{i,0}$ also shows that $E_0\to E+k\hbar\Omega$, $E_1\to V_{\rm osc}/2$, and $E_i\to 0$ for $i\geq 2$. We thus have $E(t)=E+k\hbar\Omega+V_{\rm osc}\cos(\Omega t)$ as energy for the eigenstates $\Psi_{m,j,k}^{\mathrm{III},\pm}(\mathbf{r},t)$, which is in agreement with our previous result. When N takes a finite value, one has to check how close the E_i get to the ideal values of $E_0=E+k\hbar\Omega$, $E_1=V_{\rm osc}/2$, and $E_i=0$ for $i\geq 2$.

In the applications provided in the paper, we consider for example a photon energy $\hbar\Omega$ of 0.5 eV, an amplitude $V_{\rm osc}$ of −1 eV for the oscillating barrier, and a cutoff parameter N of 12. We show in Table I how the values of λ_k and $\Sigma_{k'=-N}^{N} k'\hbar\Omega|V_{k',k}|^2$ compare with the limit of $k\hbar\Omega$ that one obtains when $N\to\infty$. The eigenstates $\Psi_{m,j,k}^{\mathrm{III},\pm}(\mathbf{r},t)$ in the anode region III turn out to have a better representation for $k=0$, while deviations in the eigenvalues λ_k and in the mean energies $\Sigma_{k'=-N}^{N} k'\hbar\Omega|V_{k',k}|^2$ appear as $|k|$ increases. These deviations can be kept under control by taking N sufficiently large. For given values of $V_{\rm osc}$ and $\hbar\Omega$, the cutoff parameter N can actually be determined by taking the first value, for which E_i that characterize the eigenstates $\Psi_{m,j,k}^{\mathrm{III},\pm}(\mathbf{r},t)$ deviate by less than 10^{-13} eV from the ideal values of $E_0=E+k\hbar\Omega$, $E_1=V_{\rm osc}/2$, and $E_i=0$ for $i\geq 2$. This condition must be fulfilled for the states with $k=0$ and 1. When $V_{\rm osc}>\hbar\Omega$, this condition must be extended to the states with $k\leq\frac{V_{\rm osc}}{\hbar\Omega}$.

APPENDIX B: EXPLICIT FORMULAS FOR THE TIME DEPENDENCE OF THE UPWARD AND DOWNWARD CURRENTS

By using the transfer-matrix methodology presented in Sec. II, one can derive solutions in the anode region III that have the following analytical expression:

$$
\Psi_{m,j,0}^{+} = \sum_{m',j',k'} S_{(m',j',k'),(m,j,0)}^{++}\Psi_{m',j',k'}^{\mathrm{III},+} \qquad \text{(B1)}
$$

with

$$
\Psi_{m',j',k'}^{\mathrm{III},+} = \frac{RJ_{m'}(k_{m',j'}\rho)\exp(im'\phi)}{\sqrt{2\int_0^R d\rho\rho[J_{m'}(k_{m',j'}\rho)]^2}} e^{i\sqrt{(2m/\hbar^2)(E+\lambda_{k'}-V_{\rm III})-k_{m',j'}^2}z}\sum_{k''=-N}^{N} V_{k'',k'} e^{-i(E+k''\hbar\Omega)t/\hbar} \qquad \text{(B2)}
$$

as the eigenstates in the anode region III (these states are discussed in Appendix A).

The z component of the current density associated with the wave function $\Psi^+_{m,j,0}$ is given by $J^+_{z;m,j,0} = \mathrm{Re}[\Psi^+_{m,j,0}{}^* \frac{\hbar}{im}\frac{d}{dz}\Psi^+_{m,j,0}]$. The upward current $I^+_{m,j,0}$ provided by the state $\Psi^+_{m,j,0}$ can then be calculated by

$$I^+_{m,j,0} = e\int_0^R d\rho\rho \int_0^{2\pi} d\phi\, J^+_{z;m,j,0} = \frac{e\hbar\pi R^2}{m}\mathrm{Re}\left[\sum_{m',j',k_1',k_2'} \sqrt{\frac{2m}{\hbar^2}(E+\lambda_{k_2'}-V_{\mathrm{III}})-k^2_{m',j'}} \times S^{++}_{(m',j',k_1'),(m,j,0)}{}^* S^{++}_{(m',j',k_2'),(m,j,0)} e^{i\Delta k_{z;m',j',k_1',k_2'}z} \times \sum_{k_1'',k_2''} V^*_{k_1'',k_1'} V_{k_2'',k_2'} e^{i(k_1''-k_2'')\Omega t}\right] \tag{B3}$$

with e as the absolute value of the electronic charge and

$$\Delta k_{z;m',j',k_1',k_2'} = \sqrt{\frac{2m}{\hbar^2}(E+\lambda_{k_2'}-V_{\mathrm{III}})-k^2_{m',j'}} - \sqrt{\frac{2m}{\hbar^2}(E+\lambda_{k_1'}-V_{\mathrm{III}})-k^2_{m',j'}}. \tag{B4}$$

The density of states $\mathcal{D}_{m,j,0}(E)$ that correspond to $\Psi^+_{m,j,0}$ is given by[25]

$$\mathcal{D}_{m,j,0}(E) = \frac{m}{\pi^2\hbar^2R^2}\frac{1}{\sqrt{\frac{2m}{\hbar^2}(E-V_{\mathrm{I}})-k^2_{m,j}}}, \tag{B5}$$

so that the upward current that corresponds to the full set of possible incident states in the cathode region I is given by

$$I^+ = \int_{V_{\mathrm{I}}}^{\infty}\sum_{m,j} f_{\mathrm{I}}(E)[1-f_{\mathrm{III}}(\bar{E}^{\mathrm{III}}_{m,j,0})]\mathcal{D}_{m,j,0}(E) I^+_{m,j,0} dE, \tag{B6}$$

where f_{I} and f_{III} are the Fermi factors in regions I and III and $\bar{E}^{\mathrm{III}}_{m,j,0}$ is the mean energy of the transmitted part of the state $\Psi^+_{m,j,0}$ [see Eq. (11)].

Replacing $\mathcal{D}_{m,j,0}(E)$ and $I^+_{m,j,0}$ by their respective expressions, we finally obtain

$$I^+ = \frac{2e}{h}\int_{V_{\mathrm{I}}}^{\infty}\sum_{m,j} f_{\mathrm{I}}(E)[1-f_{\mathrm{III}}(\bar{E}^{\mathrm{III}}_{m,j,0})]\mathcal{I}^+_{m,j,0} dE, \tag{B7}$$

with

$$\mathcal{I}^+_{m,j,0} = \mathrm{Re}\left[\sum_{m',j',k_1',k_2'} \frac{\sqrt{\frac{2m}{\hbar^2}(E+\lambda_{k_2'}-V_{\mathrm{III}})-k^2_{m',j'}}}{\sqrt{\frac{2m}{\hbar^2}(E-V_{\mathrm{I}})-k^2_{m,j}}} \times S^{++}_{(m',j',k_1'),(m,j,0)}{}^* S^{++}_{(m',j',k_2'),(m,j,0)} e^{i\Delta k_{z;m',j',k_1',k_2'}z} \times \sum_{k_1'',k_2''} V^*_{k_1'',k_1'} V_{k_2'',k_2'} e^{i(k_1''-k_2'')\Omega t}\right]. \tag{B8}$$

The term $e^{i(k_1''-k_2'')\Omega t}$ in Eq. (B8) is ultimately responsible for the time dependence of the upward current I^+. Since k_1'' and k_2'' both range from $-N$ to N, the factor $(k_1''-k_2'')$ will range from $2N$ to $2N$ so that the Fourier expansion of I^+ will actually have the form

$$I^+ = \sum_{k=-2N}^{2N} I^+_k e^{ik\Omega t}, \tag{B9}$$

where the I^+_k are the Fourier coefficients of I^+.

One can obtain the I^+_k by identifying the terms in Eqs. (B7) and (B8) that exhibit a $e^{ik\Omega t}$ dependence. For example, the term I_0 corresponds to $k_1''=k_2''$. We can then use the fact that $\Sigma_{k_1''} V^*_{k_1'',k_1'} V_{k_1'',k_2'} = \delta_{k_1',k_2'}$ and we finally obtain

$$I^+_0 = \frac{2e}{h}\int_{V_{\mathrm{I}}}^{\infty}\sum_{m,j} f_{\mathrm{I}}(E)[1-f_{\mathrm{III}}(\bar{E}^{\mathrm{III}}_{m,j,0})] \times \sum_{m',j',k'} \frac{\sqrt{\frac{2m}{\hbar^2}(E+\lambda_{k'}-V_{\mathrm{III}})-k^2_{m',j'}}}{\sqrt{\frac{2m}{\hbar^2}(E-V_{\mathrm{I}})-k^2_{m,j}}} |S^{++}_{(m',j',k'),(m,j,0)}|^2 dE, \tag{B10}$$

which is equivalent to Eq. (9).

In the general case, we have

$$I^+_k = \frac{2e}{h}\int_{V_{\mathrm{I}}}^{\infty}\sum_{m,j} f_{\mathrm{I}}(E)[1-f_{\mathrm{III}}(\bar{E}^{\mathrm{III}}_{m,j,0})]\mathcal{I}^+_{m,j,0;k} dE, \tag{B11}$$

with

$$\mathcal{I}^+_{m,j,0;k} = \sum_{m',j',k_1',k_2'} \frac{1}{2}\frac{\sqrt{\frac{2m}{\hbar^2}(E+\lambda_{k_2'}-V_{\mathrm{III}})-k^2_{m',j'}}}{\sqrt{\frac{2m}{\hbar^2}(E-V_{\mathrm{I}})-k^2_{m,j}}} \left[S^{++}_{(m',j',k_1'),(m,j,0)}{}^* S^{++}_{(m',j',k_2'),(m,j,0)} e^{+i\Delta k_{z;m',j',k_1',k_2'}z} \sum_{k_1'',k_2''} V^*_{k_1'',k_1'} V_{k_2'',k_2'} \delta_{k_1''-k_2'',k} + S^{++}_{(m',j',k_1'),(m,j,0)} S^{++}_{(m',j',k_2'),(m,j,0)}{}^* e^{-i\Delta k_{z;m',j',k_1',k_2'}z} \sum_{k_1'',k_2''} V_{k_1'',k_1'} V^*_{k_2'',k_2'} \delta_{k_2''-k_1'',k}\right]. \tag{B12}$$

The relations (B4), (B11), and (B12) lead to an important property $I_k^{+*}=I_{-k}^{+}$, which guarantees that the current I^+ is real valued. The summations in all the formulas presented in this appendix must only include propagative states.[33]

The time dependence of the downward current can be obtained in a similar way. The main difference is that the cathode region I is the transmission region and that the anode region III is the region of incidence. We therefore use S^{--} instead of S^{++} and exchange V_{III} with V_{I} in the preceding formulas. Since $V_{\mathrm{osc}}(\mathbf{r})=0$ in region I, we have also $\lambda_k=k\hbar\Omega$ and $V_{k',k}=\delta_{k',k}$, which reduces the complexity of the expressions relevant to the downward current I^-.

*Corresponding author; alexandre.mayer@fundp.ac.be

[1] T. E. Sullivan, P. H. Cutler, and A. A. Lucas, Surf. Sci. **54**, 561 (1976).
[2] K. H. Evenson, G. W. Day, J. S. Wells, and L. O. Mullen, Appl. Phys. Lett. **20**, 133 (1972).
[3] W. Krieger, T. Suzuki, M. Volcker, and H. Walther, Phys. Rev. B **41**, 10229 (1990).
[4] N. M. Miskovsky, S. H. Park, P. H. Cutler, and T. E. Sullivan, J. Vac. Sci. Technol. B **12**, 2148 (1994).
[5] K. M. Evenson, J. S. Well, F. R. Peterson, B. L. Danielson, G. W. Day, R. L. Barger, and J. L. Hall, Phys. Rev. Lett. **29**, 1346 (1972).
[6] Proceedings of the 17th General Conference on Measures and Weights (Comptes Rendus, BIPM, Sevres, France, 1983), p. 93.
[7] P. Gueret, A. Baratoff, and E. Marclay, Europhys. Lett. **3**, 367 (1987).
[8] P. H. Cutler, T. E. Feuchtwang, T. T. Tsong, H. Nguyen, and A. A. Lucas, Phys. Rev. B **35**, 7774 (1987).
[9] H. Q. Nguyen, P. H. Cutler, T. E. Feuchtwang, Z.-H. Huang, Y. Kuk, P. J. Silverman, A. A. Lucas, and T. E. Sullivan, IEEE Trans. Electron Devices **36**, 2671 (1989).
[10] T. E. Sullivan, Y. Kuk, and P. H. Cutler, IEEE Trans. Electron Devices **36**, 2659 (1989).
[11] T. E. Hartman, J. Appl. Phys. **33**, 3427 (1962).
[12] L. O. Hocker, D. R. Sokoloff, V. Daneu, A. Szoke, and A. Javan, Appl. Phys. Lett. **12**, 401 (1968).
[13] J. F. Mulligan, Am. J. Phys. **44**, 960 (1976).
[14] J. Terrien, Rep. Prog. Phys. **39**, 1067 (1976).
[15] C. Fumeaux, W. Herrmann, F. K. Kneubuhl, and H. Rothuizen, Infrared Phys. Technol. **39**, 123 (1998).
[16] N. Beverini, G. Carelli, E. Ciaramella, G. Contestabile, A. De Michele, and M. Presi, Laser Phys. **15**, 1334 (2005).
[17] E. Bava, N. Beverini, G. Carelli, A. De Michele, G. Galzerano, E. Maccioni, A. Moretti, M. Prevedelli, F. Sorrentino, and C. Svelto, IEEE Trans. Instrum. Meas. **54**, 1407 (2005).
[18] A. A. Lucas, A. Moussiaux, M. Schmeits, and P. H. Cutler, Commun. Phys. (London) **2**, 169 (1977).
[19] N. M. Miskovsky, S. J. Shepherd, P. H. Cutler, T. E. Sullivan, and A. A. Lucas, Appl. Phys. Lett. **35**, 560 (1979).
[20] A. Mayer, M. S. Chung, B. L. Weiss, N. M. Miskovsky, and P. H. Cutler, Phys. Rev. B **77**, 085411 (2008).
[21] R. H. Good and E. W. Müller, in *Handbuch der Physik*, edited by S. Flugge (Springer-Verlag, Berlin, 1956), Vol. 21, p. 176.
[22] F. H. M. Faisal, *Theory of Multiphoton Processes* (Plenum, New York, 1987), pp. 8–10.
[23] Th. Laloyaux, I. Derycke, J.-P. Vigneron, Ph. Lambin, and A. A. Lucas, Phys. Rev. B **47**, 7508 (1993).
[24] A. Mayer and Ph. Lambin, Nanotechnology **16**, 2685 (2005).
[25] A. Mayer and J.-P. Vigneron, Phys. Rev. B **56**, 12599 (1997).
[26] A. Mayer and J.-P. Vigneron, Phys. Rev. E **59**, 4659 (1999).
[27] A. Mayer and J.-P. Vigneron, Phys. Rev. E **60**, 7533 (1999).
[28] A. Mayer and J.-P. Vigneron, Phys. Rev. E **61**, 5953 (2000).
[29] A. Mayer and J.-P. Vigneron, Phys. Rev. B **62**, 16138 (2000).
[30] A. Mayer, N. M. Miskovsky, and P. H. Cutler, Phys. Rev. B **65**, 195416 (2002).
[31] A. Pimpale, S. Holloday, and R. J. Smith, J. Phys. A **24**, 3533 (1991).
[32] B. F. Bayman and C. J. Mehoke, Am. J. Phys. **51**, 875 (1983).
[33] M. Büttiker, Y. Imry, R. Landauer, and S. Pinhas, Phys. Rev. B **31**, 6207 (1985).
[34] H. Tamura and T. Ando, Phys. Rev. B **44**, 1792 (1991).
[35] P. J. Price, Microelectron. J. **30**, 925 (1999).
[36] T. E. Sullivan, P. H. Cutler, and A. A. Lucas, Surf. Sci. **62**, 455 (1977).